

CHAPTER 25

NONDESTRUCTIVE TESTING

Robert L. Crane
Theodore E. Matikas
Air Force Wright Laboratory
Materials Directorate
Nondestructive Evaluation Branch
WL/MLLP
Wright Patterson Air Force Base
Dayton, Ohio

25.1 INTRODUCTION	729	25.5.2 The Impedance Plane	746
25.2 LIQUID PENETRANTS	730	25.5.3 Liftoff of the Inspection Coil from the Specimen	747
25.2.1 The Penetrant Process	730	25.6 THERMAL METHODS	750
25.2.2 Categories of Penetrants	730	25.6.1 Infrared Cameras	750
25.2.3 Reference Standards	730	25.6.2 Thermal Paints	751
25.2.4 Limitations of Penetrant Inspections	730	25.6.3 Thermal Testing	751
25.3 ULTRASONIC METHODS	732	25.7 MAGNETIC PARTICLE METHOD	751
25.3.1 Sound Waves	733	25.7.1 The Magnetizing Field	751
25.3.2 Reflection and Transmission of Sound	733	25.7.2 Continuous versus Noncontinuous Fields	752
25.3.3 Refraction of Sound	735	25.7.3 The Inspection Process	753
25.3.4 The Inspection Process	737	25.7.4 Demagnetizing the Part	753
25.4 RADIOGRAPHY	738	APPENDIX A ULTRASONIC PROPERTIES OF COMMON MATERIALS	754
25.4.1 The Generation and Absorption of X Radiation	739	APPENDIX B ELECTRICAL RESISTIVITIES AND CONDUCTIVITIES OF COMMERCIAL METALS AND ALLOYS	759
25.4.2 Neutron Radiography	740		
25.4.3 Attenuation of X Radiation	741		
25.4.4 Film-Based Radiography	742		
25.4.5 The Penetrameter	743		
25.4.6 Real-Time Radiography	744		
25.4.7 Computed Tomography	744		
25.5 EDDY CURRENT INSPECTION	746		
25.5.1 The Skin Effect	746		

25.1 INTRODUCTION

Nondestructive evaluation (NDE) encompasses those physical and chemical tests that are used to determine if a component or structure can perform its intended function without the test methods impairing the component's performance. Until recently, NDE was relegated to detecting physical flaws and estimating their dimensions. These data were used to determine if a component should be scrapped or repaired, based on quality-acceptance criteria. Such traditional definitions are being expanded as requirements for high-reliability, cost-effective NDE tests are increasing. In addition, NDE techniques are changing as they become an integral part of the automated manufacturing process.

This chapter is but a brief review of the more commonly used NDE methods. Those who require more detailed information on standard NDE practices should consult Refs. 1–6 at the end of the chapter. For information on recent advances in NDE research the reader is referred to Refs. 7–14.

The NDE methods reviewed here consist of the five classical techniques—penetrants, ultrasonic methods, radiography, magnetic particle tests, and eddy current methods. Additionally, we have briefly covered thermal-inspection methods.

25.2 LIQUID PENETRANTS

Liquid penetrants are used to detect surface-connected discontinuities in solid, nonporous materials. The method uses a brightly colored penetrating liquid that is applied to the surface of a clean part. The liquid in time enters the discontinuity and is later withdrawn to provide a surface indication of the flaw. This process is depicted schematically in Fig. 25.1. A penetrant flaw indication in turbine blade is shown in Fig. 25.2.

25.2.1 The Penetrant Process

Technical societies and military specifications have developed classification systems for penetrants. Society documents (typically ASTM E165) categorize penetrants into two methods (visible and fluorescent) and three types (water washable, post-emulsifiable, and solvent removable). Penetrants, then, are classified by type of dye, rinse process, and sensitivity. See Ref. 1, Vol. 2, for a more detailed discussion of penetrant testing.

The first step in penetrant testing (PT) or inspection is to clean the part (Fig. 25.1*a* and 25.1*b*). Many times this critical step is the most neglected phase of the inspection. Since PT detects only flaws that are open to the surface, the flaw and part surface must, prior to inspection, be free of dirt, grease, oil, water, chemicals, and other foreign materials. Typical cleaning procedures use vapor degreasers, ultrasonic cleaners, alkaline cleaners, or solvents.

After the surface is clean, a penetrant is applied to the part by dipping, spraying, or brushing. Step 2 in Fig. 25.1*c* shows the penetrant on the part surface and in the flaw. In the case of tight surface openings, such as fatigue cracks, the penetrant must be allowed to remain on the part for a minimum of 30 minutes to enhance the probability of complete flaw filling. Fluorescent dye penetrants are used for many inspections where high sensitivity is required.

At the conclusion of the minimum dwell time, the penetrant on the surface of the part is removed by one of three processes, depending on the characteristics of the inspection penetrant. Ideally, only the surface penetrant is removed and the penetrant in the flaw is left undisturbed (Fig. 25.1*c*).

The final step in a basic penetrant inspection is the application of a developer, wet or dry, to the part surface. The developer aids in the withdrawal of penetrant from the flaw and provides a suitable background for flaw detection. The part is then viewed under a suitable light source; either ultraviolet or visible light. White light is used for visible penetrants while ultraviolet light is used for fluorescent penetrants. A typical penetrant indication for a crack in a jet engine turbine blade is shown in Fig. 25.2.

25.2.2 Categories of Penetrants

Once the penetrant material is applied to the surface of the part, it must be removed before an inspection can be carried out. Penetrants are often categorized by their removal method. There are generally three methods of removing the penetrant and thus three categories. Water-washable penetrants contain an emulsifier that permits water to wet the penetrant and carry it from the part, much as a detergent removes stains from clothing during washing. The penetrant is usually removed with a water spray. Post-emulsifiable penetrants require that an emulsifier be applied to the part to permit water to remove the excess penetrant. After a short dwell time, during which the emulsifier mixes with the surface penetrant, a water spray cleans the part. For solvent-removable penetrants, the excess material is usually removed with a solvent spray and wiping. This process is generally used in field applications where water-removal techniques are not applicable.

25.2.3 Reference Standards

Several types of reference standards are used to check the effectiveness of liquid-penetrant systems. One of the oldest and most often-used methods involves chromium-cracked panels, which are available in sets containing fine, medium, and coarse cracks. The panels are capable of classifying penetrant materials by sensitivity and identifying changes in the penetrant process.

25.2.4 Limitations of Penetrant Inspections

The major limitation of liquid-penetrant inspection is that it can only detect flaws that are open to the surface. Other methods are used for detecting subsurface flaws. Another factor that may inhibit the effectiveness of liquid-penetrant inspection is the surface roughness of the part being inspected. Very rough surfaces are likely to produce excessive background or false indications during inspection. Although the liquid-penetrant method is used to inspect some porous parts, such as powder metallurgy

Table 25.1 Capabilities of the Common NDE Methods

Method	Typical Flaws Detected	Typical Application	Advantages	Disadvantages
Radiography	Voids, porosity, inclusions, and cracks	Castings, forgings, weldments, and structural assemblies	Detects internal flaws; useful on a wide variety of geometric shapes; portable; provides a permanent record	High cost; insensitive to thin laminar flaws, such as tight fatigue cracks and delaminations; potential health hazard
Liquid penetrants	Cracks, gouges, porosity, laps, and seams open to a surface	Castings, forgings, weldments, and components subject to fatigue or stress-corrosion cracking	Inexpensive; easy to apply; portable; easily interpreted	Flaw must be open to an accessible surface, level of detectability operator-dependent
Eddy current testing	Cracks, and variations in alloy composition or heat treatment, wall thickness, dimensions	Tubing, local regions of sheet metal, alloy sorting, and coating thickness measurement	Moderate cost, readily automated; portable	Detects flaws that change in conductivity of metals; shallow penetration; geometry-sensitive
Magnetic particles	Cracks, laps, voids, porosity, and inclusions	Castings, forgings, and extrusions	Simple; inexpensive; detects shallow subsurface flaws as well as surface flaws	Useful for ferromagnetic materials only; surface preparation required, irrelevant indications often occur; operator-dependent
Thermal testing	Voids or disbonds in both metallic and nonmetallic materials, location of hot or cold spots in thermally active assemblies	Laminated structures, honeycomb, and electronic circuit boards	Produces a thermal image that is easily interpreted	Difficult to control surface emissivity; poor discrimination
Ultrasonic testing	Cracks, voids, porosity, inclusions and delaminations and lack of bonding between dissimilar materials	Composites, forgings, castings, and weldments and pipes	Excellent depth penetration; good sensitivity and resolution; can provide permanent record	Requires acoustic coupling to component; slow; interpretation is often difficult

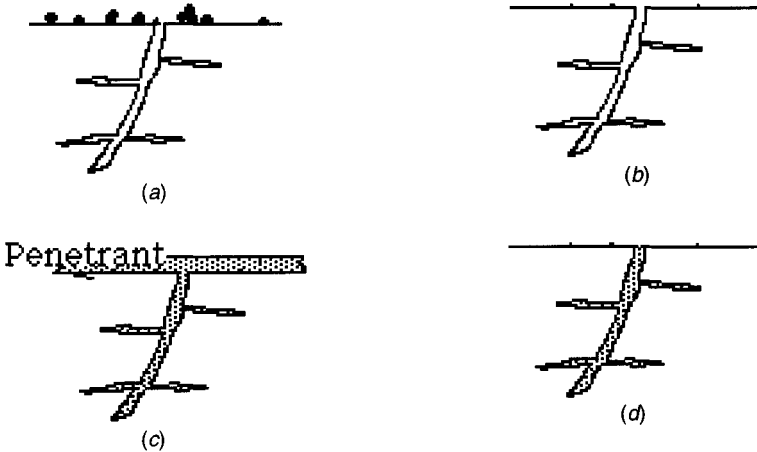


Fig. 25.1 (a) Schematic representation of a part surface before cleaning for penetrant inspection; (b) part surface after cleaning and before penetrant application; (c) part after penetrant application; (d) part after excess penetrant has been removed.

parts, the process generally is not well suited for the inspection of porous materials because the background penetrant from pores obscures flaw indications.

25.3 ULTRASONIC METHODS

Ultrasonic methods utilize sound waves to inspect the interior of materials. Sound waves are mechanical or elastic waves and are composed of oscillations of discrete particles of the material. The process of inspection using sound waves is quite analogous to the use of sonar to detect schools of fish or map the ocean floor. Both government and industry have developed standards to regulate ultrasonic inspections. These include, but are not limited to, the American Society for Testing and Materials Specifications 214-68, 428-71, and 494-75, and military specification MIL-1-8950H. Acoustic and ultrasonic testing takes many forms, from simple coin-tapping to transmission of sonic waves into a material and analyzing the returning echoes for the information they contain about its internal structure. Reference 15 provides an exhaustive treatment of this inspection technique.

Instruments operating in the frequency range between 20 and 500 kHz are usually defined as sonic instruments, while above 500 kHz is the domain of ultrasonic methods. In order to generate and receive the ultrasonic wave, a piezoelectric transducer is usually used to convert electrical signals

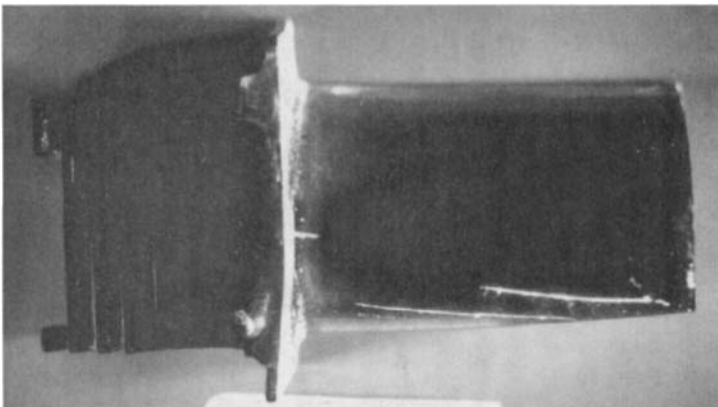


Fig. 25.2 Penetrant indication of a crack running along the edge of a jet engine turbine blade. Ultraviolet light causes the extracted penetrant to glow.

to sound wave signals and vice versa. This transducer usually consists of a piezoelectric crystal mounted in a waterproof housing that facilitates its electrical connection to a pulsar (transmitter) receiver. In the transmit mode, a high-voltage, short-duration pulse of electrical energy is applied to the crystal, causing it to change shape rapidly and emit a high-frequency pulse of acoustic energy. In the receive mode, any ultrasonic waves or echoes returning from the acoustic path, which includes the coupling media and part, compress the piezoelectric crystal, producing an electrical signal that is amplified and processed by the receiver.

25.3.1 Sound Waves

Ultrasonic waves have several characteristics, such as wavelength (λ), frequency (f), velocity (v), pressure (P), and amplitude (a). The following relationship between wavelength, frequency, and sound velocity is valid for all types of waves

$$f \times \lambda = v$$

For example, the wavelength of longitudinal ultrasonic waves of frequency 2 MHz propagating in steel is 3 mm and the wavelength of shear waves is 1.6 mm.

The sound pressure is related to the particles' amplitude by the relation, where the terms were defined in the previous paragraph.

$$P = 2\pi f \times \rho \times v \times a$$

Ultrasonic waves are reflected from all interfaces/boundaries that separate media with different acoustic impedances, a phenomenon quite similar to the reflection of electrical signals in transmission lines. The acoustic impedance Z of any medium capable of supporting sound waves is defined by

$$Z = \rho \times v$$

where ρ = the density of the medium in g/cm^3

v = the velocity of sound along the direction of propagation

Materials with high acoustic impedance are called (sonically) hard in contrast with (sonically) soft materials. For example, steel ($Z = 7.7 \text{ g/cm}^3 \times 5.9 \text{ km/sec} = 45.4 \times 10^6 \text{ kg/m}^2 \text{ sec}$) is sonically harder than aluminum ($Z = 2.7 \text{ g/cm}^3 \times 6.3 \text{ km/sec} = 17 \times 10^6 \text{ kg/m}^2 \text{ sec}$). An extensive list of acoustic properties of many common materials is provided in Appendix A.

25.3.2 Reflection and Transmission of Sound

Since very nearly all the acoustic energy incident on air/solid interfaces is reflected because of the large impedance mismatch of these two media, a coupling medium with an impedance closer to that of the part is needed to transmit ultrasonic energy into the part under examination. A liquid couplant has obvious advantages for components with complex external geometries, and water is the couplant of choice for most inspection situations. The receiver, in addition to amplifying the returning echoes, also time-gates echoes that return between the front surface and rear surfaces of the component. Thus, any unusually occurring echo can either be displayed separately or used to set off an alarm.

A schematic diagram of a typical ultrasonic pulse echo setup is shown in Fig. 25.3. This display of voltage amplitude versus time or depth (if acoustic velocity is known) at a single point of the specimen is known as an A-scan. In the setup shown in Fig. 25.3, the first signal corresponds to the reflection of the ultrasonic wave from the front surface of the sample (FS), the last signal corresponds to the reflection of the ultrasonic wave from the back surface of the sample (BS), and the signal in between corresponds to the defect echo from inside the component.

The portion of sound energy that is reflected from or transmitted through each interface is a function of the impedances of media on each side of the interface. The reflection coefficient R (ratio of the sound pressures or intensities of the reflected and incident waves) and transmission coefficient T (ratio of the sound pressures or intensities of the transmitted and incident waves) for an acoustic wave normally incident onto an interface are

$$R = \frac{p_r}{p_i} = \frac{Z_1 - Z_2}{Z_1 + Z_2}$$

$$R_{pwr} = \frac{I_r}{I_i} = \left(\frac{Z_1 - Z_2}{Z_1 + Z_2} \right)^2$$

Likewise, the transmission coefficients, T and T_{pwr} , are defined as

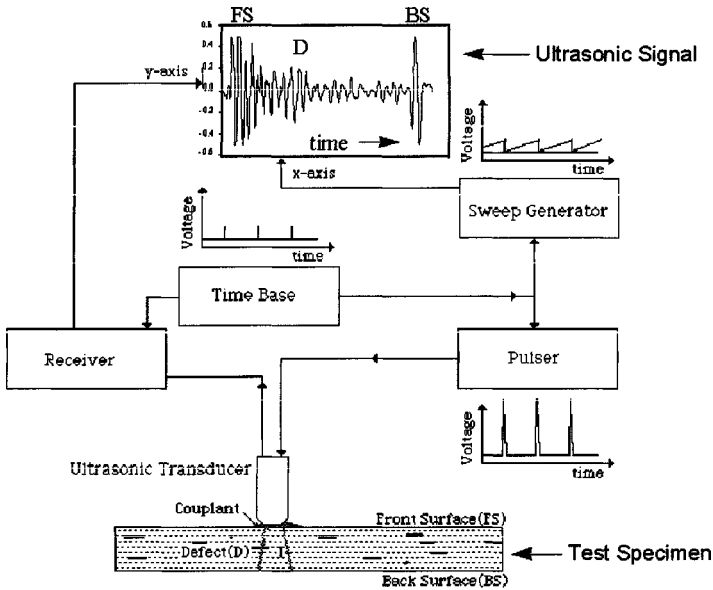


Fig. 25.3 Schematic representation of ultrasonic data collection and display in the A-scan mode.

$$T = \frac{p_t}{p_i} = \frac{2Z_{II}}{Z_I + Z_{II}}$$

$$T_{pwr} = \frac{I_t}{I_i} = \frac{4 \frac{Z_{II}}{Z_I}}{\left(1 + \frac{Z_{II}}{Z_I}\right)^2}$$

where I_i , I_r , and I_t = the incident, reflected, and transmitted acoustic field intensities, respectively
 Z_I = the acoustic impedance of the medium from which the sound is incident
 Z_{II} = the acoustic impedance into which the wave is transmitted.

From these equations, it is apparent that for a crack like flaw containing air, $Z_I = 450 \text{ kg/cm}^2 \text{ sec}$, located in, say, a piece of steel, $Z_{II} = 45.4 \times 10^6 \text{ kg/m}^2 \text{ sec}$, the reflection coefficient for the flaw is practically -1.0 . The minus sign indicates a phase change of 180° for the reflected pulse (note that the defect echo signal in Fig. 25.3 is inverted or phase shifted 180° from the front surface signal).

Effectively no acoustic energy is transmitted across an air gap, necessitating the use of water as a coupling medium in ultrasonic testing. The acoustic properties of several common materials are shown in Appendix A. These data are useful for a number of simple, yet informative, calculations.

Thus far, the discussion has involved only longitudinal waves. This type of wave motion is the only type that can travel through fluids such as air and water. This wave motion is quite similar to the motion one would observe in a spring, or a Slinky toy, where the displacement and wave motion are collinear (the oscillations occur in the direction of wave propagation). This wave is also called compressional or dilatational since compressional and dilatational forces are active in it. Audible sound waves transmitting acoustic energy from a source through the air to our ears are compressional waves. This mode of wave propagation is supported in liquids and gases as well as in solids. However, a solid medium can also support other modes of wave propagation, such as shear waves, Rayleigh or surface waves, and so on. Shear or transverse waves have a wave motion that is analogous to the motion one gets by snapping a rope; that is, the displacement of the rope is perpendicular to the direction of wave propagation. The velocity of this wave mode is about one-half that of compressional

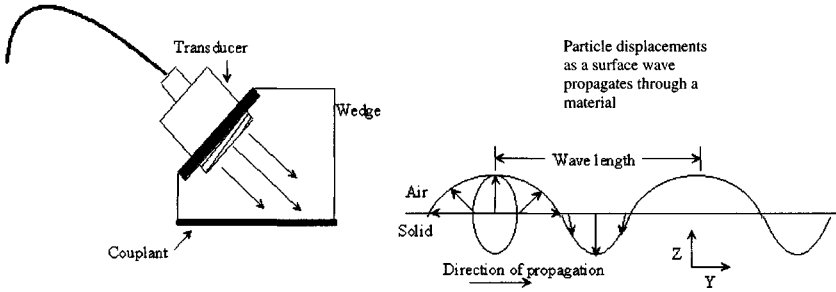


Fig. 25.4 Generation and propagation of surface waves in a material.

waves and is only supported by solid media, as shown in Appendix A. Shear waves can be generated when a longitudinal wave is incident on a fluid/solid interface at angles of incidence other than 0°. Rayleigh or surface waves have elliptical wave motion, as shown in Fig. 25.4, and about one ultrasonic wavelength penetration in the material. Therefore, they are used to detect surface and very near-surface flaws. The velocity of Rayleigh waves is about 90% of the shear wave velocity. Their generation requires a special device, as shown in Fig. 25.4, which enables an incident ultrasonic wave on the sample at a specific angle that is characteristic of the material (Rayleigh angle). See Ref. 15 for more details.

25.3.3 Refraction of Sound

The direction of propagation of acoustic waves is described by the acoustic equivalent of Snell’s law. Referring to Fig. 25.5, the directions of propagation are determined with the following equation:

$$\frac{\sin \theta_i}{c_1} = \frac{\sin \theta_r}{c_r} = \frac{\sin \gamma_r}{b_r} = \frac{\sin \theta_t}{c_t} = \frac{\sin \gamma_t}{b_t}$$

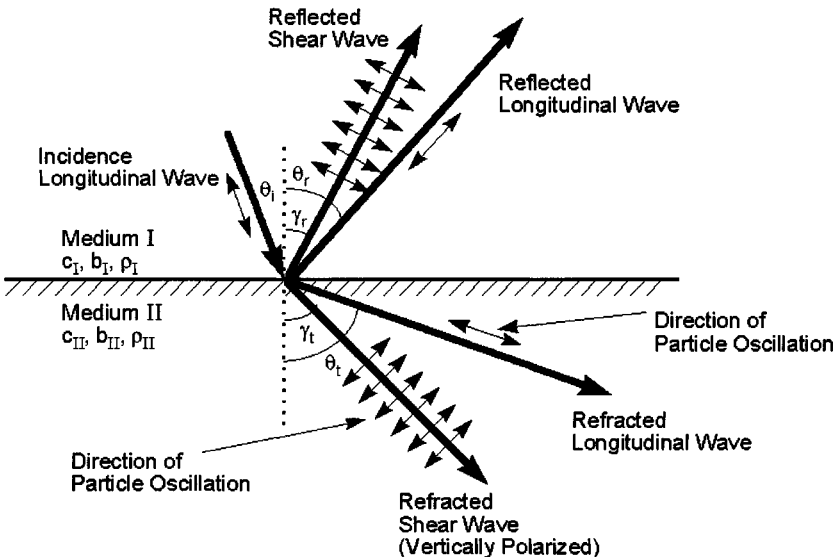


Fig. 25.5 Schematic representation of Snell’s law and the mode conversion of a longitudinal wave incident on a solid–solid interface.

where c_1 = the velocity of the incident longitudinal wave
 c_r and b_r = the velocities of the longitudinal and shear reflected waves
 c_t and b_t = the velocities of the longitudinal and shear transmitted waves in the solid II

In the case of steel/water interface, there are no shear reflected waves and the above relationship is simplified. Since the water has a lower wave speed than either the compressional or shear wave speeds of the steel, the acoustic waves in the metal are refracted toward from the normal. The situation changes dramatically if the order of the media is changed to a water/steel interface. In this case, the wave speed of the water is less than either the shear or longitudinal wave speed of the steel. With a longitudinal wave incident from water at an angle other than 90° both longitudinal and shear waves are generated in the steel and travel away from the interface at angles greater than the incident wave. This effect can be predicted using Snell's law. Using the previous equation and the wave speeds of steel from Appendix A the reader will note that the longitudinal wave is refracted further from the normal than the shear wave. As the angle of incidence is increased, there will be an angle where the longitudinal wave is refracted parallel to the surface or simply propagates along the interface. This angle is called the first critical angle. If the angle of incidence is increased further, there will be a point where the shear wave also disappears. This angle is called the second critical angle. A computer-drawn curve is shown in Fig. 25.6, in which the normalized acoustic energy reflected and refracted at a water/steel interface are plotted as a function of angle of incidence. Note that the longitudinal or first critical angle for steel occurs at 14.5° . Likewise, second critical angle occurs at 30° . If the angle of incidence is increased above the first critical angles, then only a shear wave is generated in the metal and propagates at an angle of refraction determined by Snell's law. Angles of incidence above the second critical angle produce a complete reflection of the incident acoustic waves—that is, no acoustic energy enters the solid. At a specific angle of incidence (Rayleigh angle), surface acoustic waves are generated on the material. The Rayleigh angle can be easily calculated from Snell's law when the refraction angle is 90° . The Rayleigh angle for steel occurs at 29.5° . Between the two critical angles, only the shear wave is present in the material. In this region, shear wave testing is performed, which has two advantages. First, with only one type of wave present, the

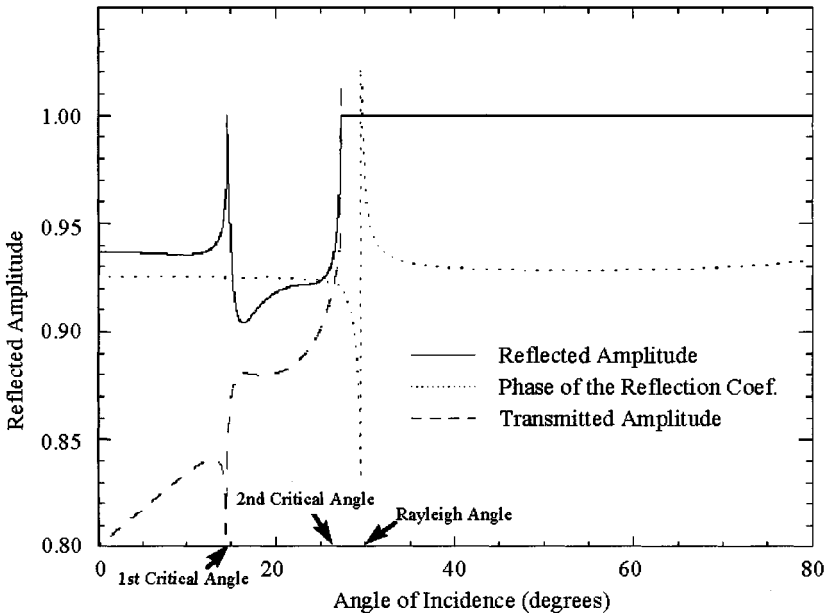


Fig. 25.6 Amplitude (energy flux) and phase of the reflected coefficient and transmitted amplitude vs. angle of incidence for a longitudinal wave incident on a water-steel interface. The arrows indicate the critical angles for the interface.

ambiguity that would exist concerning where a reflected wave originates is not present. Second, the lower wave speed of the shear wave means that about twice the time is available for resolving distances within the part under examination. These advantages mean shear wave inspection is often chosen for inspection of thin metallic structures, such as those in aircraft.

Using only Snell's law and the relationships for the reflection and transmission coefficients, a great deal of information can be deduced about any ultrasonic inspection situation in which the acoustic wave is incident at 90° to the surface. For other angles of incidence or for a component containing one or more thin layers, a computer program is used to analyze the acoustic interactions. For more complicated materials or structures, such as fiber-reinforced composites, any analytical predictions require computer computation for even relatively simple situations. In these cases, more complicated modes of wave propagation occur, such as Lamb waves (plate waves), Stoneley waves (interface waves), Love waves (guided in layers of a solid material coated onto another one), and so on.

25.3.4 The Inspection Process

Once the type of inspection has been chosen and the optimum experimental parameters have been determined, it remains only to choose the mode of presentation of the data. If the size of the flaw is small compared to the transducer, then the A-scan method can be chosen, as shown in Fig. 25.3. The acquisition of a series of A-scans obtained by scanning the transducer in one dimension (line) is called a B-scan. In the A-scan mode, the voltage output of the transducer is displayed versus time or depth in the part. The size of the flaw is often inferred by comparing the size of the defect signal to a set of standard calibration blocks, which have varying sizes of flat bottom holes drilled in one end. For a specific transducer, the magnitude of the signal from the flat bottom hole is an increasing function of hole diameter. In this way, an equivalent flat-bottom-hole size can be given for a flaw signal obtained from a defect in a component. The equivalent size is meaningful only for flaws that are nearly perpendicular to the ultrasonic signal path.

If the flaw size is larger than the transducer or if a number of flaws are expected, then the C-scan mode is usually selected. In this inspection mode, as shown in Fig. 25.7, the transducer is scanned back and forth in two coordinates across the part. When a flaw signal is detected between the front and back surface signals, then a line of intersection of the raster-scan with the flaw is left blank on a piece of paper or CRT screen. In this manner, a planar projection of each flaw is viewed and its positional relationships to others and to the part boundaries are easily assessed. Unfortunately, in this mode the depth information for each flaw is frequently lost; therefore, this mode is mostly used for thin, layered aircraft structures. However, if the ultrasonic signals are monitored at a particular time window (time gate), an image can be obtained. This C-scan can represent various characteristics of the ultrasonic signal detected in the particular time gate, such as peak-to-

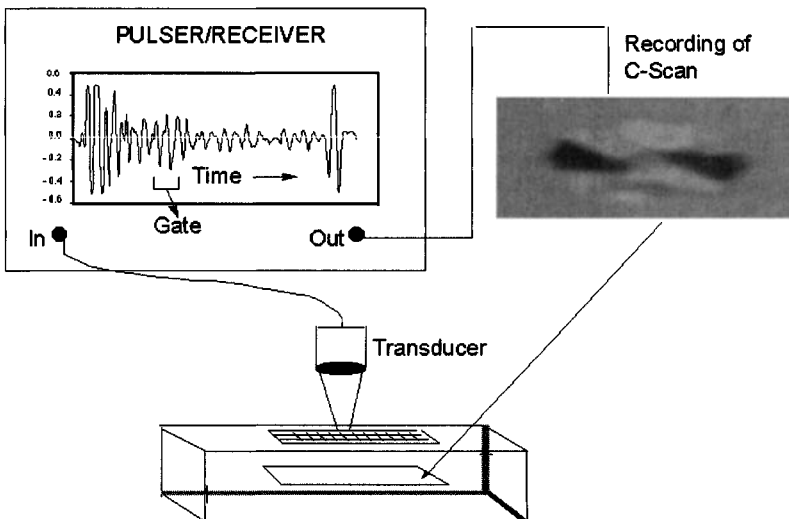


Fig. 25.7 Schematic representation of ultrasonic data collection. The data are displayed using the C-scan mode. The image shows a defect located at a certain depth in the material.

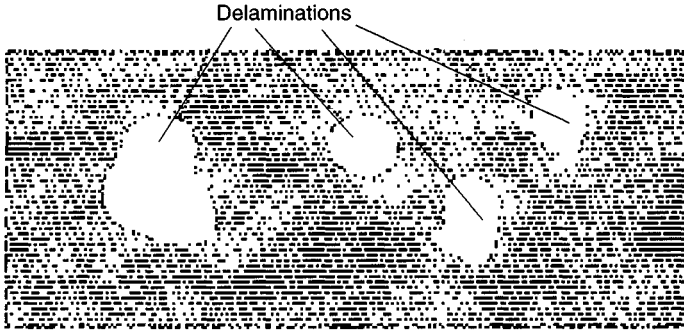


Fig. 25.8 Typical C-scan image of composite specimen, showing delaminations and porosity.

peak amplitude, positive or negative peaks, time of flight, mean value of amplitude, and so on. The C-scan provides a visual representation of a slice of the material at a certain depth and is very useful for nondestructive inspection.

Depending on the structural complexity and the attenuation of the signal by the material and electronic instrumentation, flaws as small as 0.015 in., in one dimension, can be reliably detected and quantified using this ultrasonic method. An example of a typical C-scan printout of an adhesively bonded test panel is shown in Fig. 25.8. While the panel was fabricated with Teflon void-simulating implants, the numerous white areas indicate the presence of a great deal of porosity in the adhesive. For a much more extensive treatment of this inspection technique, see Ref. 1, Vol. 7.

25.4 RADIOGRAPHY

Radiography is an NDE method in which the projected X-ray attenuation for many straight line paths through a specimen are recorded as a two-dimensional image on recording medium. For a more detailed description of radiography testing, see Ref. 1, Vol. 3.

This process, shown schematically in Fig. 25.9, records visually any feature that changes the attenuation of the X-ray beam along the path that the X-ray photons take through the structure. This local change in attenuation produces a change in the density or darkness of the film or electronic recording device at that location. This change in brightness, which is sometimes a mere shadow, is used by the inspector to detect internal anomalies. In this task, the inspector is greatly aided in detecting and quantifying flaws by knowing the geometry of the part and how this relates to the

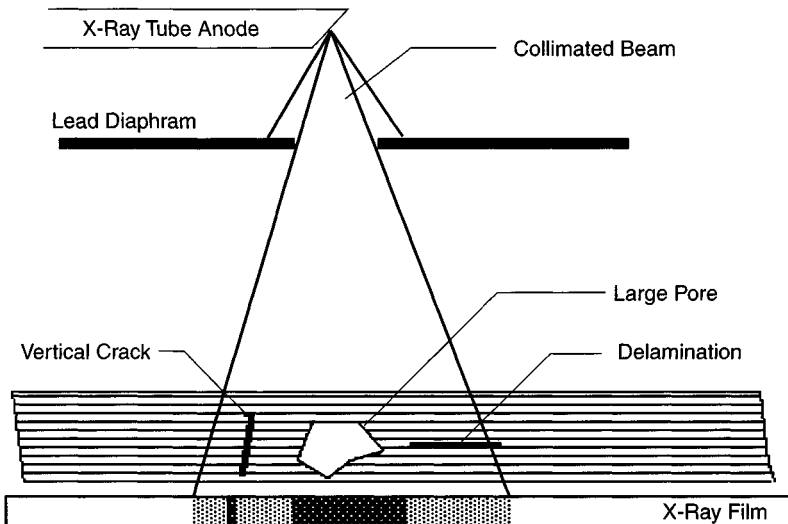


Fig. 25.9 Schematic radiograph of a thin plate with two types of flaws.

image. It should be noted in Fig. 25.9 that only flaws that change the attenuation of the X-ray beam on passage through the part are recorded. For example, a delamination in a composite or laminated material that is not the result of missing material is not visible because there is no change in attenuation of the X-ray beam. Flaws that are oriented perpendicular to the plate do attenuate the X-ray beam as much as adjacent beam paths and therefore are easily detected as a darkened line or area on the film. An example of a crack in the correct orientation to be visible on a radiograph of a piece of tubing is shown in Fig. 25.10.

25.4.1 The Generation and Absorption of X Radiation

X radiation can be produced via a number of processes. The most common way of producing X rays is with an electron tube in which a beam of energetic electrons impact a metal target. As the electrons are rapidly decelerated in this collision, a wide band of X radiation is produced, analogous to white light. This is referred to as Bremsstrahlung or braking radiation. Higher-energy electrons produce shorter-wavelength or more energetic X rays. The relationship between the shortest-wavelength X radiation produced and the highest voltage applied to the tube is given by

$$\lambda = \frac{12,336}{\text{voltage}}$$

where λ = the shortest wavelength of the X radiation-produced in Ångstroms.

The more energetic the radiation, the more penetrating power it has. Therefore, higher-energy radiation is used on dense materials, such as metals. While it is possible to analytically predict what X-ray energy would provide the best image for a specific material and geometry, a simpler method of arriving at the optimum X-ray energy is to use the curves shown in Fig. 25.11. Note that high-energy radiation is used for dense materials, such as steels, or for thick, less dense materials, such as large composite solid rocket motors. An alternative to Fig. 25.11 is the table of radiographic equivalence factors shown in Table 25.2.¹⁶ Aluminum is the standard material for voltages below 100 Kv, while steel is the standard above this voltage. When radiographing another material its thickness is multiplied by the equivalency factor, of Table 25.2, to obtain the equivalent thickness of the standard material to obtain an acceptable radiograph. For example, if one needed to produce a radiograph of a 0.75-in.-thick piece of brass with a 400-Kv X-ray source, one would multiply the 0.75 by the factor of 1.3 to obtain 0.98. This means that an acceptable radiograph of the brass plates would be obtained with the same exposure parameters as would be used for 0.98 in. (approximately 1 in.) of steel.

Penetrating radiation for radiography can also be obtained from the decay of radioactive sources. This is usually referred to as gamma radiation. These radiation sources have distinct characteristics that distinguish them from X-ray tubes. First, gamma radiation is very nearly monochromatic; that is, the radiation spectrum contains only one or two dominant characteristic energies. Second, the energies of most sources are in the million volt range, making them ideal for inspecting highly attenuated materials and structures. Third, the small size of these sources permits them to be used in situations where an X-ray tube could not fit into a small space. Fourth, since the gamma-ray source is continually decaying, adjustments to the exposure time must be made in order to achieve consistent results over time. Finally, the operator must be cognizant that the source is always on and is therefore

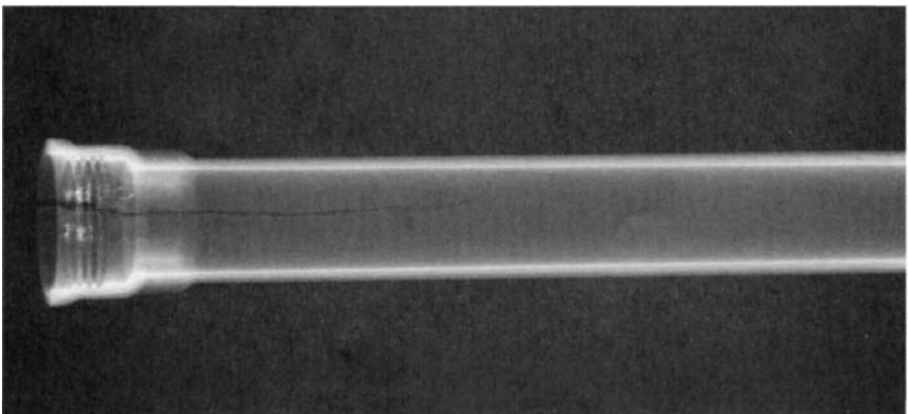


Fig. 25.10 Radiograph of an aluminum tubing with a crack.

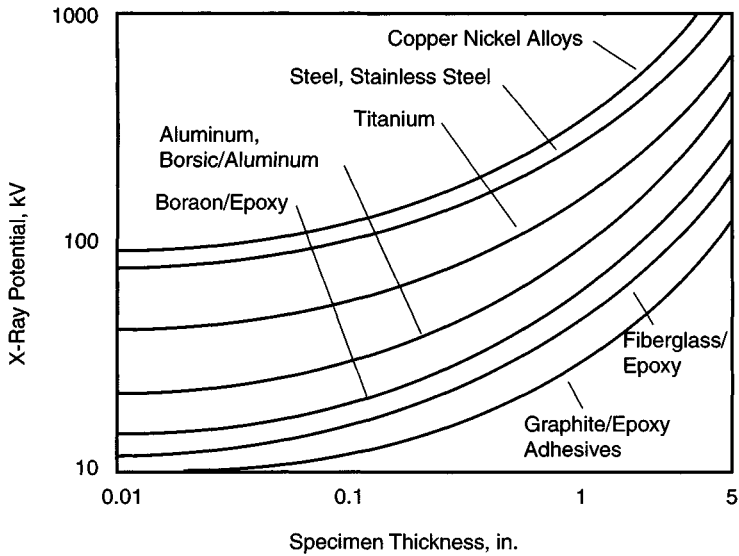


Fig. 25.11 Plot of the X-ray tube voltage vs. thickness for several important industrial materials.

a constant safety hazard. Since, in use, gamma radiography differs little from standard practice with X-ray tubes, we will make no further distinction between the two.

25.4.2 Neutron Radiography

Neutron radiography¹⁷ is useful for inspecting materials and structures in specialized circumstances. The attenuation of neutrons is not related to atomic number in a smooth manner as it is with X-rays. While x-radiation is most heavily absorbed by high atomic number elements, this is not true of neutrons as shown in Fig. 25.12. The reader can easily discern that hydrogen adsorbs neutrons to a greater extent than do most metals. This means that hydrogen containing materials could be detected

Table 25.2 Radiographic Equivalence Factors

Energy Level	100 kV	150 kV	220 kV	250 kV	400 kV	1 MeV	2 MeV	4-25 MeV	192Ir	60Co
<i>Metal</i>										
Magnesium	0.05	0.05	0.08							
Aluminum	0.08	0.12	0.18						0.35	0.35
Aluminum alloy	0.10	0.14	0.18						0.35	0.35
Titanium		0.54	0.54		0.71	0.9	0.9	0.9	0.9	0.9
Iron/all steels	1.0	1.0	1.0	1.0	1.0	1.0	1.0	1.0	1.0	1.0
Copper	1.5	1.6	1.4	1.4	1.4	1.1	1.1	1.2	1.1	1.1
Zinc		1.4	1.3		1.3			1.2	1.1	1.0
Brass		1.4	1.3		1.3	1.2	1.1	1.0	1.1	1.0
Inconel X		1.4	1.3		1.3	1.3	1.3	1.3	1.3	1.3
Monel	1.7		1.2							
Zirconium	2.4	2.3	2.0	1.7	1.5	1.0	1.0	1.0	1.2	1.0
Lead	14.0	14.0	12.0			5.0	2.5	2.7	4.0	2.3
Halfnium			14.0	12.0	9.0	3.0				
Uranium			20.0	16.0	12.0	4.0		3.9	12.6	3.4

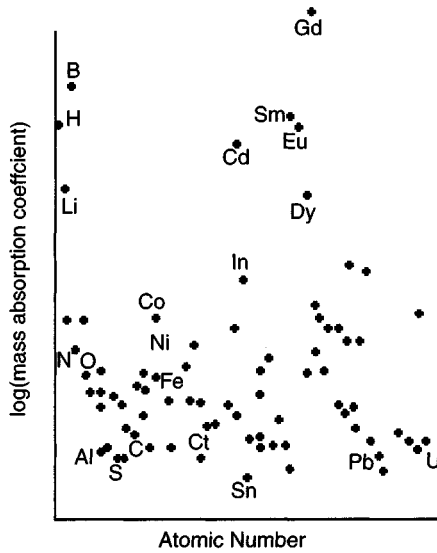


Fig. 25.12 A plot of neutron mass absorption coefficient vs. atomic number.

inside a metal container. Neutron radiography can be used to detect adhesive flaws in bonded metal structures because the hydrogen containing adhesive absorbs more neutrons than the metal structure—see the schematic representation of a neutron radiograph of an adhesively bonded specimen with various flaws shown in Fig. 25.13.

Neutron radiography, however, does have several constraints. First, neutrons do not expose radiographic film and therefore fluorescing materials are often used to produce an image or screens. The image produced in this manner is not as sharp and well-defined as one produced with X rays. Second, there does not exist a suitable portable source of neutrons, which means that a nuclear reactor is used to supply the penetrating radiation. Even with these restrictions, there are times when there is no other alternative to neutron radiography and the utility of the method outweighs its expense and difficulty of usage.

25.4.3 Attenuation of X Radiation

The interpretation of a radiograph requires some fundamental understanding of the X-ray absorption. The basic relationship governing this phenomenon is

$$I = I_0 e^{-\mu x}$$

where I and I_0 = the transmitted and incident X-ray beam intensities, respectively

μ = the attenuation coefficient of the material in cm^{-1}

x = the thickness of the specimen, in cm

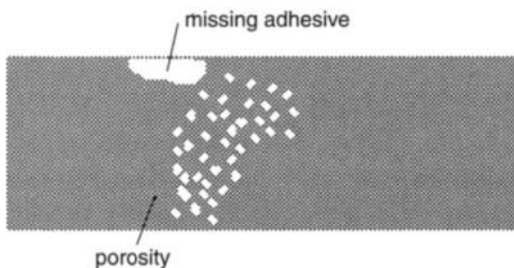


Fig. 25.13 Idealized neutron radiograph of bonded aluminum panel with two types of flaws.

Since the attenuation coefficient is a function of both the composition of the specimen and the wavelength of the X rays, it must be calculated or measured for each inspection. It is possible to calculate the attenuation coefficient of a material for a specific X-ray energy using the mass absorption coefficient, μ_m , as defined below. The mass absorption coefficients for most elements are readily available for a variety of X-ray energies. (Ref. 1, Vol. 3, pp. 836–878)

$$\mu_m = \frac{\mu}{\rho}$$

where μ_m = the attenuation coefficient of a specific element, in reciprocal cm
 ρ = its density in g/cm³

If the mass absorption coefficient for each element, is multiplied by its weight fraction in the material and these quantities summed, one obtains the mass absorption coefficient of the material. Multiplying this quantity by the density of the material yields its attenuation coefficient. This procedure is not often used in practice because the results are valid for a narrow band of wavelengths. In practice, radiographic equivalency factors are used instead. This procedure points out that each element in a material contributes to the attenuation coefficient by an amount proportional to its percentage of the composition.

25.4.4 Film-Based Radiography

The classical method of recording an X-ray image is with film. However, new solid state X-ray area detectors permits the recording of X-ray images electronically. Both of these recording mechanisms utilize similar mathematical relationships to describe their sensitivity to defects. These will be covered next from the standpoint of film.

The relationship between the darkness on an X-ray film and the quantity of radiation falling on it is shown in Fig. 25.14. This is a log-log plot of darkness or film density and relative exposure. Relative exposure may be varied by changing either the time of exposure, intensity of the beam or specimen thickness. The slope of the curve along its linear portion is referred to as the film gamma, γ . Film has characteristics that are quite analogous to electronic devices. For example, the greater the gamma or amplification capability of the film, the smaller its dynamic range—range of exposures over which thickness changes in part will be accurately recorded. If it is desirable to use a high gamma film to detect subtle flaws in a part with several thicknesses, then the radiographer will frequently use two different film types in the same cassette—see Fig. 25.15. In this way, each film will be optimum for the different thicknesses of the part.

It is possible to calculate the minimum detectable flaw size for a specific radiographic inspection. Additionally, a method is available to check the radiographic procedure to determine if the radiograph was taken in a manner that the smallest flaws are detectable. In sensitivity calculations a small flaw is represented by a small change in thickness of the part. Whether a defect is detectable depends on the correct alignment of the flaw with respect to the X-ray source and film. The following calculation

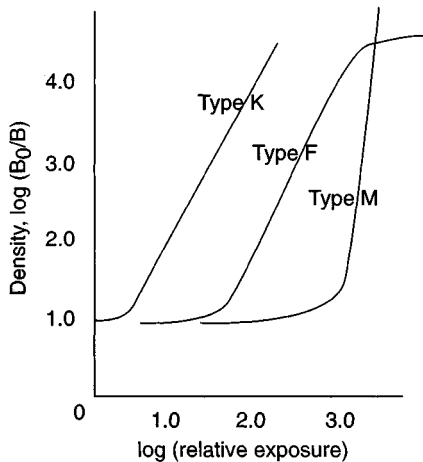


Fig. 25.14 Density or darkness of X-ray film vs. relative exposure for three common radiography films.

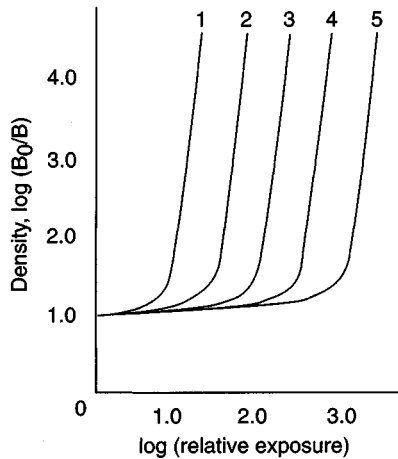


Fig. 25.15 Density vs. relative exposure for films that could be used in a multiple film exposure to obtain optimum flaw detectability in a complex part.

only is an estimation of the best sensitivity of the radiographic process to small changes in part thickness.

Using a knowledge of the minimum density difference that is detectable by the average radiographic inspector, the following relationship can be derived that relates the radiographic sensitivity, *S*, in percent to thickness changes to film and specimen parameters:

$$S = \frac{2.3}{\gamma \times \mu \times x}$$

- where γ = the film gamma for the exposure conditions used
- μ = the attenuation coefficient of the specimen
- x = the maximum thickness of the part being inspected

25.4.5 The Penetrameter

The radiographic process is usually checked with a small device called a penetrameter that is shown schematically in Fig. 25.16. Its image on a radiograph is shown schematically in Fig. 25.17. The penetrameter is a thin strip of metal in which three holes of varying sizes are machined. It is composed of the same material as the specimen under inspection and has a thickness either 1%, 2%, or 4% of the maximum thickness of the part. The holes in the penetrameter have diameters that are 1, 2, and 4 times the thickness of the penetrameter. The sensitivity achieved for each radiographic can be easily determined by noting the smallest hole just visible in the thinnest penetrameter on a film and referring to Table 25.3. Using the formula for sensitivity and then noting if that level was achieved in practice, the radiographic process can be quantitatively controlled. While this procedure does not offer any guarantee of detecting flaws, it is quite useful in controlling the mechanics of the inspection.

Other variables of the radiographic process may also be easily and rapidly changed with the aid of tables, graphs, and nomograms, which are usually provided by film manufacturers free of charge. For more information in this regard, see the commercial literature.

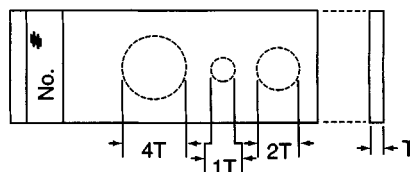


Fig. 25.16 Schematic of typical X-ray penetrameter.

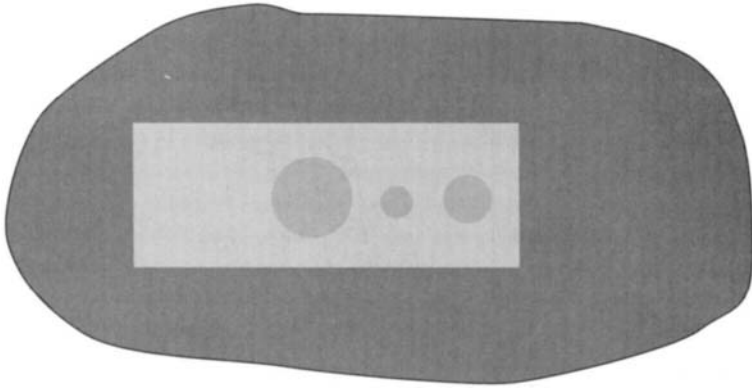


Fig. 25.17 Idealized radiograph of the penetrator shown in Fig. 25.16. The 1T hole is just visible, indicating the resolution obtained in the radiograph.

25.4.6 Real-Time Radiography

While film radiography represents the bulk of the radiographic NDE performed at this time, new methods of both recording the data and analyzing it are rapidly becoming accepted. For example, filmless radiography (FR) uses solid-state detectors or television detection and image-processing methods instead of film to record the image. These methods have several advantages along with some disadvantages. For example, real time radiography (RTR) or FR permits the viewing of a radiographic image while the specimen is being moved. This often permits the detection of flaws that would normally be missed in conventional film radiography because of the limited number of views or exposures usually taken. The price to be paid for these advantages can be the lower resolution of the FR system when compared to film. Typical resolution capabilities of an FR system are in the range from 4 to perhaps 12 line pairs/mm, while film has resolution capabilities in the range from 10–100 line pairs/mm. This means that some types of very fine flaws are not detectable with FR and the inspector must resort to film. Another factor that must be considered when comparing these two methods is the possibility of digital image processing, which is easily implemented with FR systems. These methods can be of enormous benefit in enhancing flaws that might otherwise be invisible to the inspector. While the images on film can also be enhanced using the same image-processing schemes, they cannot be performed in real or near real time, as can be done with an electronic system.

25.4.7 Computed Tomography

Another advance in industrial radiography that promises to have a major impact on the interaction of NDE with engineering design and analysis is computed tomography (CT). CT produces an image of a thin slice of the specimen under examination. This slice is parallel to the path of the X-ray beam as it passes through the specimen as contrasted to classical radiography, wherein the image is formed on a plane perpendicular to the path of the X-ray beam on passage through the specimen. While the classical radiographic image is difficult to interpret because it represents a collapse of all of the images of the specimen between the source of X rays and the recording media, the CT image appears as a thin slice of the specimen.

Table 25.3

Sensitivity, S (%)	Quality Level (% T—Hole Diameter)
0.7	1—1T
1.0	1—2T
1.4	2—1T
2.0	2—2T
2.8	2—4T
4.0	4—2T

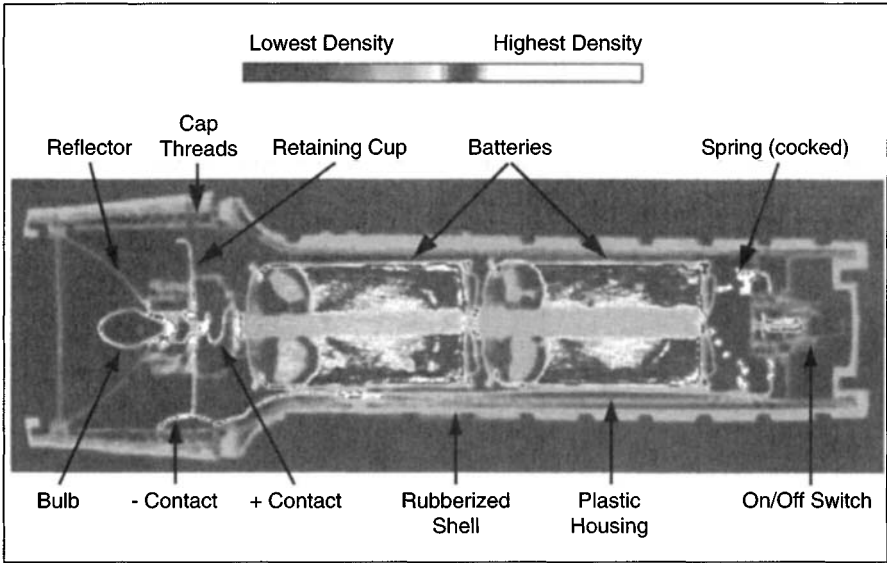


Fig. 25.18 Computed tomograph of flashlight.

This comparison is best explained with actual images from these two modalities. Figure 25.10 shows a typical industrial radiograph where one can easily see the image of the top and bottom surfaces of the tube. Contrast this with the image in Fig. 25.18, which shows CT slice through a flashlight. The individual components of the flashlight are easily visible and defects in its assembly could be easily detected. An image in even finer detail than this that shows the microstructural details of a material is shown in Fig. 25.19. Everyone will recognize that this is a pencil. Not only are the

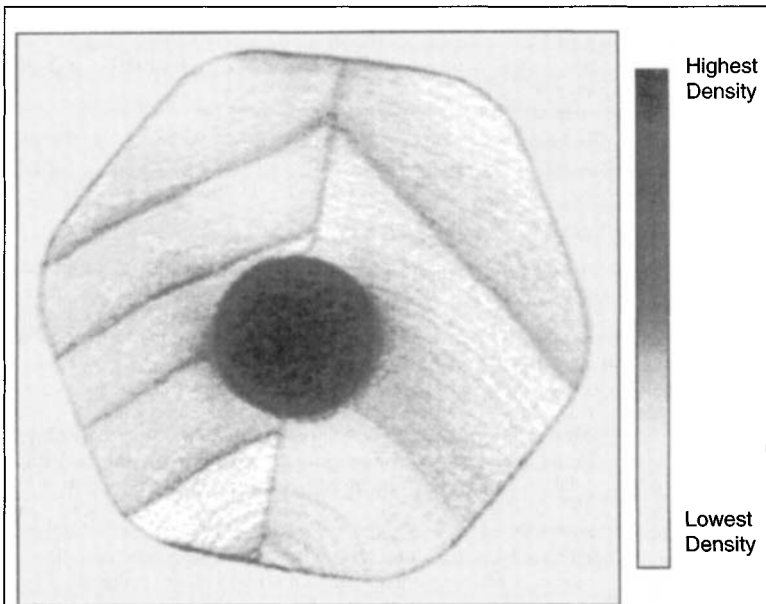


Fig. 25.19 Computed tomograph of a pencil. Note the yearly growth rings in wood.

key features clearly visible, but even the growth rings of the wood are clearly visible. In fact, the details of the growth during each season are visible as rings within rings. The information in the CT image contrasted with conventional radiographs is striking. First, the detectability of a defect is independent of its position in the image. Second, the defect detectability is very nearly independent of its orientation. This is not the case with classical radiography. The extent to which CT will alter radiographic NDE is only now being realized. It is possible to link the digital CT image with finite element analysis software to examine precisely how the flaws present within the cross section affect such parameters as the stress distribution and heat flow. With little effort, one could analyze the full three-dimensional performance of many engineering structures.

25.5 EDDY CURRENT INSPECTION

Eddy current (EC) methods are used to inspect electrically conducting components for flaws, such as surface connected and near-surface cracks and voids; heat-treatment; external dimensions and thickness of thin metals; and thickness of nonconducting coatings on a metal substrate. Quite often, several of these conditions can be monitored simultaneously if instrumentation capable of measuring the phase of the eddy current signal is used.

This NDE method is based on the principle that eddy currents are induced in a conducting material when a coil or array of conductors (probe) with an alternating or pulsed electric current is placed in close proximity to its surface. The induced currents create an electromagnetic field that opposes the field of the inducing coil in accordance with Lenz's law. The eddy currents circulate in the part in closed, continuous paths, and their magnitude depends on the following variables: the magnitude and frequency of the current in the inducing coil; the coil's shape and position relative to the surface of the part; the electrical conductivity, magnetic permeability, and shape of the part; and the presence of discontinuities or inhomogeneities within the material. Therefore, the eddy currents are useful in measuring the properties of materials and detecting discontinuities or variations in geometry of components.

25.5.1 The Skin Effect

Since alternating currents are necessary to perform this type of inspection, information from the inspection is limited to the near-surface region by the skin effect. Within the material, the eddy current density decreases exponentially with the depth. The density of the eddy current field falls off exponentially with depth and diminishes to a value of about 37% of the at-surface value at a depth referred to as the standard depth of penetration (SDP). The SDP, in meters, can be calculated with the simple formula

$$SDP = \frac{1}{\sqrt{\pi f \sigma \mu}}$$

where f = the test frequency in Hz

σ = the test material's electrical conductivity in mho/m (see Appendix B for a table of conductivities for common metals)

μ = its permeability in H/m

This latter quantity is the product of the relative permeability of the specimen, 1.0 for nonmagnetic materials, and the permeability of free space, which is 4×10^{-7} H/m.

25.5.2 The Impedance Plane

While the SDP is used to give an indication of the depth from which useful information can be obtained, the choice of the independent variables in most test situations is usually made using the impedance plane diagram suggested by Förster.¹⁸ It is theoretically possible to calculate the optimum inspection parameters from numerical codes based on Maxwell's equations, but this is a laborious task that is justified only in special situations.

The eddy currents induced at the surface of a material are time-varying and have amplitude and phase. The complex impedance of the coil used in the inspection of a specimen is a function of a number of variables. The effect of changes in these variables can be conveniently displayed with the impedance diagram, which shows variations in the amplitude and phase of the coil impedance as functions of the dependent variables specimen conductivity, thickness, and distance between the coil and specimen or liftoff. For the case of an encircling coil on a solid cylinder, shown schematically in Fig. 25.20, the complex impedance plane is displayed in Fig. 25.21. The reader will note that the ordinate and abscissa are normalized by the inductive reactance of the empty coil. This eliminates the effect of the geometry of the coil and specimen. The numerical values on the large curve, which are called reference numbers, are used to combine the effects of the conductivity, size of the test specimen, and the frequency of the measurement into a single parameter. This yields a diagram that is useful for most test conditions. The reference numbers shown on the outermost curve are obtained with the following relationship, for nonmagnetic materials.

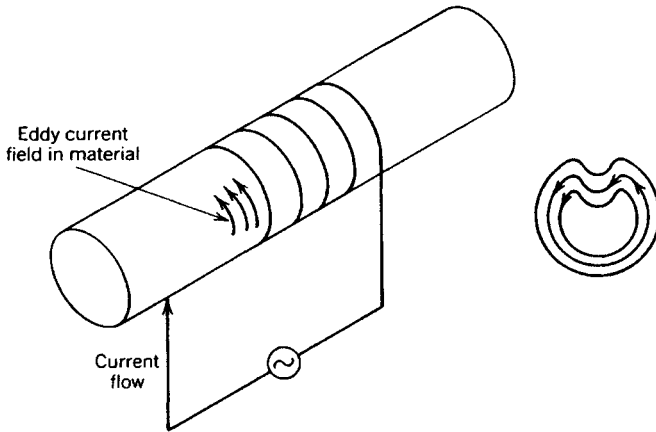


Fig. 25.20 Schematic representation of eddy current inspection of a solid cylinder. Also shown are the eddy current paths within the cross section of the cylinder in the vicinity of a crack.

$$\text{reference \#} = r\sqrt{2\pi f\mu\sigma}$$

where r = the radius of the bar in meters

f = the frequency of the test in Hz

μ = the magnetic permeability of free space (4×10^{-7} H/m)

σ = the conductivity of the specimen in mho/m

The outer curve in Fig. 25.21 is useful only for the case where the coil is the same size as the solid cylinder under test. For those cases where the coil is larger than the test specimen, a coil filling factor must be calculated and the appropriate point on a new curve located. This is easily accomplished using the fill factor N of the coil, which is defined as

$$N = \left(\frac{\text{diameter}_{\text{specimen}}}{\text{diameter}_{\text{coil}}} \right)^2$$

Figure 25.21 shows the impedance plane with a curve for a specimen/coil inspection geometry with a fill factor of 0.75. Note that the reference numbers on the curves representing the different fill factors can be determined by projecting a straight line from 1.0 on the ordinate to the reference number of interest, as is shown for the reference number 5.0. Both the fill factor and the reference number change when the size of the specimen or coil changes. Assume that a reference number of 5.0 is appropriate to a specific test with $N = 1.0$; if the coil diameter is changed so that the fill factor becomes 0.75, then the new reference number will be equal to $5.0 \times \sqrt{0.75} = 4.33$. While the actual change in reference number for this case follows the path indicated by the dotted line of this curve, we have estimated the change along the straight line. This yields a small error in optimizing the test setup, but is sufficient for most purposes. For a more detailed treatment of the impedance plane the reader is referred to Ref. 1, Vol. 4. The inspection geometry discussed thus far has been for a solid cylinder. The other geometry of general interest is the thin-walled tube in this case the skin effect limits the thickness of metal that may be effectively inspected.

For an infinitely thin-walled tube, the impedance plane is shown in Fig. 25.22. Also included in this figure is the curve for a solid cylinder. The dotted lines that connect these two cases are for thin-walled cylinders of varying thicknesses. The semicircular curve for the thin cylinder is used in the same manner as described above for the solid cylinder.

25.5.3 Liftoff of the Inspection Coil from the Specimen

In most inspection situations, the only independent variables are frequency and liftoff. High frequency excitations are frequently used for detecting defects, such as surface connected cracks or corrosion, while low frequencies are used to detect subsurface flaws. It is also possible to change the coil shape and measurement configuration to enhance detectability, but the discussion of these parameters is beyond the scope of this article and the reader is referred to the literature for a discussion of these more complex variables. The relationships discussed thus far may be put into application by examining a small section of Fig. 25.22. This figure is shown in expanded form in Figure 25.23. In this figure, changes in thickness, liftoff, and conductivity are represented by vectors. These vectors all

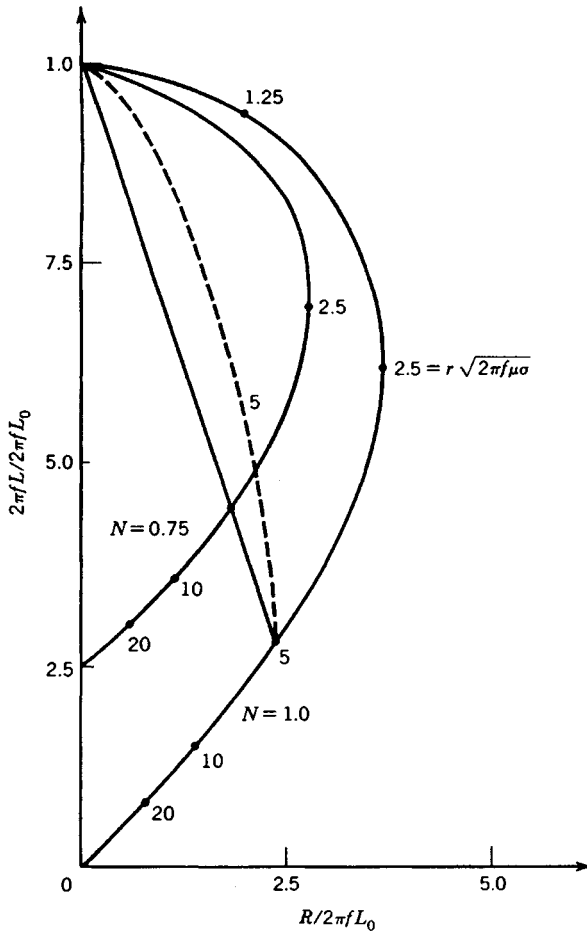


Fig. 25.21 The normalized impedance diagram for a long encircling coil on a solid, nonferromagnetic cylinder. For $N = 1$ the coil and cylinder have the same diameter; while for $N = 0.75$ the coil is approximately 1.155 times larger than the cylinder.

point in different directions representing the phase of the different possible signals. Instrumentation with phase discrimination circuitry can differentiate between these signals and therefore is often capable of detecting two changes in specimen condition at once. Changes in conductivity can arise from several different conditions. For example, aluminum alloys can have different conductivities depending on their heat treatment. Changes in apparent conductivity are also due to the presence of cracks or voids. A crack decreases the apparent conductivity of the specimen because the eddy currents must travel a longer distance to complete their circuit within the material. Lift-off and wall thinning are also shown on Fig. 25.23. Thus, two different flaw conditions can be rapidly detected. There are situations where changes in wall thickness and lift-off result in signals that are very nearly out of phase and therefore the net change is not detectable. If this situation is suspected, then inspection at two different frequencies could permit the detection of this situation. There are other inspection situations that cannot be covered in this brief description. These include the inspection of ferromagnetic alloys, plate and sheet stock, and the measurement of film thicknesses on metal substrates. For a treatment of these and other special applications of eddy current NDE, the reader is referred to Ref. 1, Vol. 4.

There are numerous methods of making eddy current NDE measurements. Two of the more common generic methods are shown schematically in Fig. 25.24. In the absolute coil arrangement, very accurate measurements can be made with the differences between the two samples. In the differential coil method, it is the differences between the two variables at two slightly different

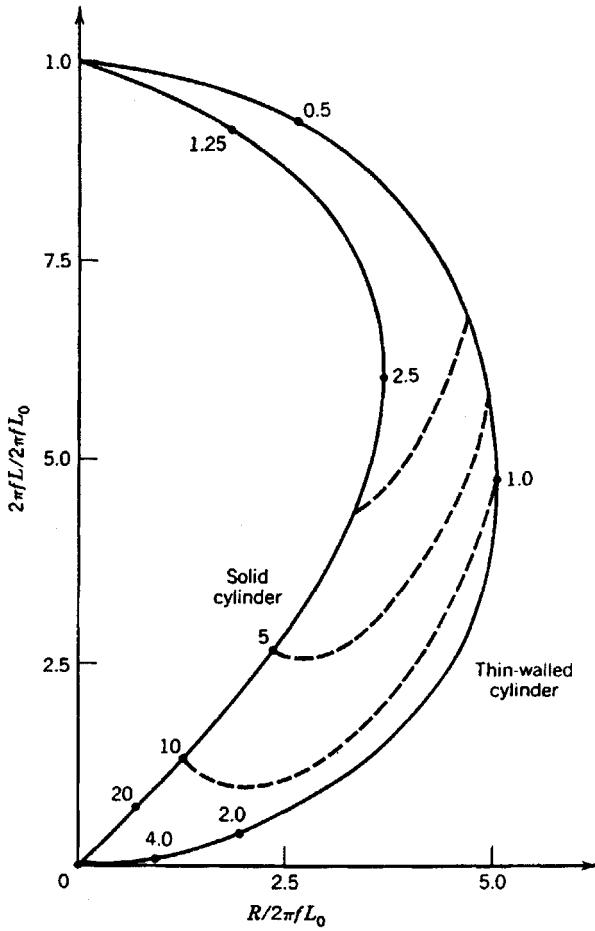


Fig. 25.22 The normalized impedance diagram for a long encircling coil on a solid and thin-walled solid, nonferromagnetic cylinders. The dashed lines represent the effects of varying wall thickness.

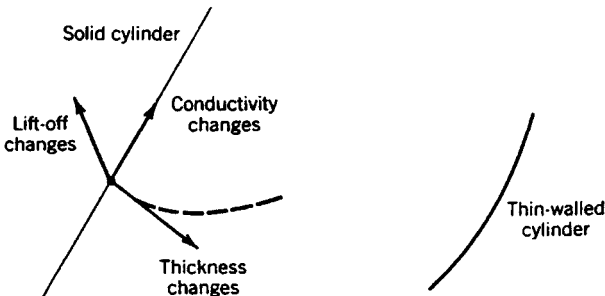


Fig. 25.23 The effects of various changes in inspection conditions on signal changes in the impedance plane of Fig. 25.22. Phase differentiation is relatively easily accomplished with current instrumentation.

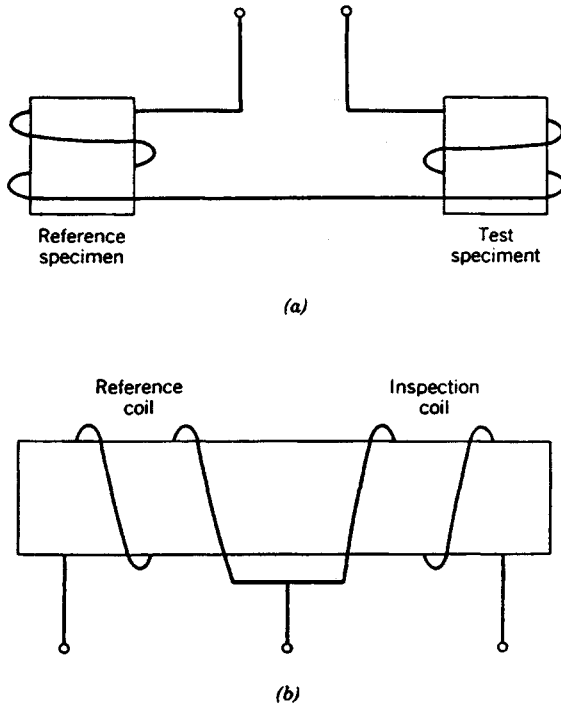


Fig. 25.24 A schematic representation of an absolute (a) versus (b) a differential coil configurations used in eddy current testing.

locations that may be detected. For this arrangement, slightly varying changes in dimensions and conductivity are not sensed, while singularities such as cracks or voids are highlighted, even in the presence of other slowly changing variables. Since the specific electronic circuitry used to accomplish this task can vary dramatically, depending on the specific inspection situation, the reader is referred to the current NDE and instrumentation literature listed in the References.

25.6 THERMAL METHODS

Thermal nondestructive test methods involve detecting either the surface or the temperature of a test object. This technique is used to detect the flow of thermal energy either into or out of a specimen, which indicate surface or near-surface defects. Other properties that can influence this NDE test are the specific heat, density, thermal conductivity, and emissivity of the test specimen. Defects that are usually detected include porosity, cracks, and laminations. The sensitivity of any thermal method is greatest for near-surface flaws and degrades rapidly for deeply buried flaws. Materials with lower thermal conductivity yield better resolution because they permit larger thermal gradients to be obtained.

25.6.1 Infrared Cameras

Infrared (IR) radiation is emitted by all objects whose temperature is above absolute zero. For objects at moderate temperatures, the thermal radiation is predominantly infrared and measurements are concentrated in the 8–14 μm wavelength region of the spectrum. IR cameras are available that view large areas by scanning over a liquid nitrogen-cooled detector. Since the IR images can be stored in digital form, further image processing is easily accomplished and permanent records can be produced. For many applications, a thermal image that reveals the relative temperature across an object is sufficient to detect near surface flaws. However, if absolute temperatures are required, the camera must be calibrated to account for the surface emissivity of the test object.

Thermography's ability to detect flaws is significantly affected by the type of flaw and its orientation with respect to the surface of the object. To have a maximum effect on the surface temperatures, the flaw must interrupt heat flow to the surface. Since a flaw can occur at any angle to the surface, the important parameter is the projected area of the flaw in the field of view of the camera.

Subsurface flaws, such as cracks parallel to the surface, porosity, and debonding of a surface layer, are easily detected. Cracks that are perpendicular to the object surface can present an infinitesimal area to the camera and therefore are very difficult to detect using thermography.

Many other NDE methods can provide better spatial resolution than thermal methods, due to spreading of thermal energy as it diffuses to the surface of the specimen. The greatest advantage to thermography is that it is a noncontact, remote technique requiring only line-of-sight access IR camera based on an object. Large areas can be viewed rapidly since scan rates for IR cameras run between 16 and 30 frames per second. Temperature differences of 0.02°C or less can be detected in a controlled environment.

25.6.2 Thermal Paints

A number of contact thermal methods are available to provide temperature or temperature-distribution data for surfaces. These methods involve applying a coating to the sample and observing the coating change color as the object is thermally cycled. Several different types of coatings are available that cover a wide temperature range. Temperature-sensitive pigments in the form of paints have been made to cover a temperature range from 40°–1600°C. Thermochromic compounds and liquid crystals change color at a specific surface temperature. The advantages of these materials are the simplicity of the test and the relatively low cost if small areas are involved.

25.6.3 Thermal Testing

Excellent results may be achieved if the IR detection can be performed in a dynamic thermal environment where the transient effects of a heat or work input into the object are monitored. This enhances detection of areas where different heat transfer rates occur. Applications involving steady-state conditions are more limited. Thermography has been successfully used in several different areas of testing. In medicine it is used to detect tumors, in aircraft manufacture or maintenance it is used to detect debonding in layered structures, in the electronics industry it is used to detect poor thermal performance of circuit board components, and it is sometimes used to detect stress-induced thermal gradients around defects in dynamically loaded test samples. For more information on thermal NDE methods, see Ref. 1, Vols. 8 and 9, and Ref. 4.

25.7 MAGNETIC PARTICLE METHOD

The magnetic particle method of nondestructive testing is used to locate surface and subsurface discontinuities in ferromagnetic materials.¹ An excellent short reference for this NDE method is Ref. 2, especially chapters 10–16. This method is based on the principle that magnetic lines of force, when present in a magnetized ferromagnetic material, are distorted by changes in material continuity, such as cracks or inclusions, as shown schematically in Fig. 25.25. If the flaw is open at the surface, the flux lines bulge or escape from the surface at the site of the discontinuity. Even near-surface flaws, such as nonmagnetic inclusions, cause the same bulging of the lines of force above the surface. This distorted field, usually referred to as a leakage field, is used to reveal the presence of the discontinuity when fine magnetic particles are attracted to it. If these particles are fluorescent, then their presence at a flaw will be visible under ultraviolet light, much as penetrant indications. See Fig. 25.7. Magnetic particle inspection is used principally for all the inspection for steel components because it is fast, easily implemented, and has rather simple flaw indications. The part is usually magnetized with an electric current and then a solution containing fluorescent particles is applied. The particles that stick to the part form the indication of the flaw.

25.7.1 The Magnetizing Field

The magnetizing field may be applied in any one of a number of ways. Its function is to generate a magnetic field in the part. The application of a magnetizing force (H) generates a magnetic flux (B) in the part as shown schematically in Fig. 25.26. The magnetic flux density, B , has units of tesla or webers/m² and the strength of the magnetic field or magnetic flux intensity, H , has units of amperes/meter. Instrumentation is often calibrated in oersteds for H and gauss for B . Referring to



Fig. 25.25 Schematic representation of the magnetic lines of flux in a ferromagnetic metal near a flaw. Small magnetic particles are attracted to the leakage field associated with the flaw.

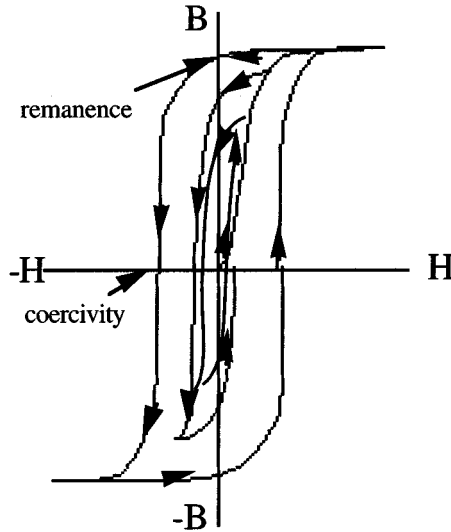


Fig. 25.26 A magnetic flux intensity, H , versus magnetic flux density, B , hysteresis curve for a typical steel. Initial magnetization starts at the origin and progresses as shown by the arrows. Demagnetization follows the arrows of the smaller hysteresis loops.

Fig. 25.26, one starts at the origin as a magnetizing force H is applied to a specimen. The magnetic field B internal to the specimen increases in a nonlinear fashion along the path shown by the arrows. If the force (H) is reversed, then the magnetic field (B) does not return to zero, but follows the arrows around the curve as shown. Note that once the magnetizing force is removed, the flux density does not return to zero, but remains at an elevated value called the material's remanence, B_r . This is where most magnetic particle inspections are performed. Also note that an appreciable reverse magnetic force $-H_c$ must be applied before the internal field density is again zero. This point $-H_c$ is referred to as the coercivity of the material. If the magnetizing force is applied and reversed while decreasing its strength, in the manner shown, then the material will respond by continually moving around this hysteresis loop.

Selection of the type of magnetizing current depends primarily on whether the defects are open to the surface or are wholly below it. Alternating current (ac) magnetizing currents are best for the detection of surface discontinuities because the current is concentrated in the near-surface region of the part. Direct current (dc) magnetizing currents are best suited for subsurface discontinuities because of the current's deeper penetration of the part. While dc can be obtained from batteries or dc generators, it is usually produced by half-wave or full-wave rectification of commercial power. Rectified current is classified as half-wave direct current (HWDC) or full-wave direct current (FWDC). Alternating current fields are usually obtained from conventional power mains, but are supplied to the part at reduced voltage, for reasons of safety and the high-current requirements of the magnetizing process.

Two general types of magnetic particles are available. One type of particle is low-carbon steel with high permeability and low retentivity, which is used dry and consists of different sizes and shapes to respond to both weak and strong leakage fields. The other type of particle consists of extremely fine particles of magnetic iron oxide that are suspended in a liquid (either a petroleum distillate or water). These particles are smaller and have a lower permeability than the dry particles. Their small mass permits them to be held by the weak leakage fields at very fine surface cracks. Magnetic particles are available in several colors to increase their contrast against different surfaces. Dry powders are typically gray, red, yellow, and black, while wet particles are usually red, black, or fluorescent.

25.7.2 Continuous versus Noncontinuous Fields

Because the field is always stronger while the magnetizing current is on, the continuous magnetizing method is generally preferred, if the part has low retentivity, the continuous method must be used. In the continuous method, the current can be applied in short pulses, typically 0.5 sec. The magnetic particles are applied to the surface during this interval and are free to move to the site of the leakage fields. In this case, the use of liquid-suspended fluorescent particles yields the most sensitive detection

method. For field inspections, the magnetizing current is usually continuously on during the test to give time for the powder to migrate to the defect site.

In the residual method, the particles are applied after the magnetizing current is removed. This method is particularly suited for production inspection of multiple parts.

The choice of direction of the magnetizing field (B) within the part involves the nature of the flaw and its direction with respect to the surface and the major axis of the part. In circular magnetization, the field runs circumferentially around the part. It is induced into the part by passing current through it between two contacting electrodes. Since only flaws perpendicular to the magnetizing lines are readily detectable, circular magnetization is used to detect flaws that are parallel or less than 45° to the surface of the part. Longitudinal magnetization is usually produced by placing the part in a coil. It creates a field running lengthwise through the part and is used to detect transverse discontinuities to the axis of the part.

25.7.3 The Inspection Process

The surface of the part to be examined should be essentially clean, dry, and free of contaminants, such as oil, grease, loose rust, loose sand, loose scale, lint, thick paint, welding flux, and weld splatter. Cleaning of the test part may be accomplished by detergents, organic solvents, or mechanical means.

Portable and stationary equipment are available. Selection of the specific type depends on the nature and location of testing. Portable equipment is available in lightweight units (35–90 lb), which can be readily taken to the inspection site. Generally, these units operate off 115, 230, or 460 V ac and supply current outputs of 750–1500 A in half-wave or ac.

25.7.4 Demagnetizing the Part

Once the inspection process is complete, the part must be demagnetized. This is done by one of several means, depending on the subsequent usage of the part. A simple way of demagnetizing the part is to do what many electronic technicians do to remove any residual magnetism from small tools. In this case, the tool is placed in the coil of a soldering iron and slowly withdrawn. This has the effect of retracing the hysteresis loop a large number of times, each time with a smaller magnetizing force applied to the tool. The tool will then have a very small remnant magnetic field that is, for all practical purposes, zero. This same process is accomplished with an industrial part by slowly reducing and reversing the magnetizing current till it is essentially zero. This process of reducing the residual magnetic field is shown schematically by following the arrows in Fig. 25.26. Another way to demagnetize the part is to heat it above the materials' Curie temperature, about 550°C for iron, where all residual magnetism disappears. This last process is the best means of removing all magnetism, but it does require the expense and time of an elevated heat treatment.

APPENDIX A

ULTRASONIC PROPERTIES OF COMMON MATERIALS

Ultrasonic Properties of Liquids

Liquid (20°C unless noted)	Longitudinal Wave Speed × 10 ⁵ cm/sec	Density gm/cm ³
Acetic Acid	1.173	1.049
Acetone	1.192	0.792
Amyl Acetate (26°C)	1.168	0.879
Aniline	0.656	1.022
Benzene	1.326	0.879
Blood (Horse) (37°C)	1.571	
Bromoform	0.928	2.890
n-Butyl Alcohol	1.268	0.810
Caprylic Acid	1.331	0.910
Carbon Disulfide	1.158	1.263
Carbon Tetrachloride	0.938	1.595
Chloroform	1.005	1.498
Formaldehyde (25°C)	1.587	0.815
Gasoline (34°C)	1.25	0.803
Glycerin	1.923	1.261
Kerosene (25°C)	1.315	0.82
Mercury	1.451	13.546
Methyl Alcohol	1.123	0.796
Oils		
Campor (25°C)	1.390	
Castor	1.500	0.969
Condenser	1.432	
Olive (22°C)	1.440	0.918
SAE 20	1.74	0.87
Sperm (32°C)	1.411	
Transformer	1.38	0.92
Oleic Acid	1.333	0.873
n-Pentane	1.044	
Silicon Tetrachloride (30°C)	0.766	1.483
Toluene	1.328	0.67
Water (distilled)	1.482	1.00
m-Xylene	1.340	0.864

Ultrasonic Properties of Solids: Metals

Metal (20°C unless noted)	Longitudinal Wave Speed × 10 ⁵ cm/sec	Transverse Wave Speed × 10 ⁵ cm/sec	Density gm/cm ³
Aluminum			
Al (1100)	6.31	3.08	2.71
Al (2014)	6.37	3.07	2.80
Al (2024-T4)	6.37	3.16	2.77
Al (2117-T4)	6.50	3.12	2.80
Al (6061-T6)	6.31	3.14	2.70
Bearing Babbit	2.30		10.1
Beryllium	12.890	8.880	1.82
Bismuth	2.18	1.10	9.80
Brass (70% Cu & 30% Zn)	4.37	2.10	8.50
Brass (Naval)	4.43	2.12	8.42

Ultrasonic Properties of Solids: Metals (Continued)

Metal (20°C unless noted)	Longitudinal Wave Speed × 10 ⁵ cm/sec	Transverse Wave Speed × 10 ⁵ cm/sec	Density gm/cm ³
Bronze (5% P)	3.53	2.32	8.86
Cadmium	2.78	1.50	8.64
Cerium	2.424	1.415	6.77
Chromium	6.608	4.005	7.20
Cobalt	5.88	3.10	8.90
Columbium	4.92	2.10	8.57
Constantan	5.177	2.625	8.88
Copper	4.759	2.325	8.93
Copper (110)	4.70	2.26	8.9
Dysprosium	2.296	1.733	8.53
Erbium	2.064	1.807	9.06
Europium	1.931	1.237	5.17
Gadolinium	2.927	1.677	7.89
Germanium	5.18	3.10	5.47
Gold	3.24	1.20	19.32
Hafnium	2.84		13.3
Hastelloy X	5.79	2.74	8.23
Hastelloy C	5.84	2.90	8.94
Holmium	3.089	1.729	8.80
Indium	2.56	0.74	7.30
Invar	4.657	2.658	
Lanthanium	2.362	1.486	6.16
Lead	2.160	0.700	11.34
Lead (96% Pb & 6% Sb)	2.16	0.81	10.88
Lutetium	2.765	1.574	9.85
Magnesium	5.823	3.163	1.74
AM-35	5.79	3.10	1.74
FS-1	5.47	3.03	1.69
J-1	5.67	3.01	1.70
M1A	5.74	3.10	1.76
O-1	5.80	3.04	1.72
Manganese	4.66	2.35	7.39
Manganin	4.66	2.35	8.40
Molybdenium	6.29	3.35	10.2
Nickel			
Pure	5.63	2.96	8.88
Inconel	5.82	3.02	8.5
Inconel (X-750)	5.94	3.12	8.3
Inconel (wrought)	7.82	3.02	8.25
Monel	5.35	2.72	8.83
Monel (wrought)	6.02	2.72	8.83
Silver-Nickel (18%)	4.62	2.32	8.75
German Silver	4.76	2.16	8.40
Neodymium	2.751	1.502	7.10
Platinum	3.96	1.67	21.4
Potassium	2.47	1.22	0.862
Praseodymium	2.639	1.437	6.75
Samarium	2.875	1.618	7.48
Silver	3.60	1.59	10.5
Sodium	3.03	1.70	0.97

Ultrasonic Properties of Solids: Metals (Continued)

Metal (20°C unless noted)	Longitudinal Wave Speed × 10 ⁵ cm/sec	Transverse Wave Speed × 10 ⁵ cm/sec	Density gm/cm ³
Steel			
1020	5.89	3.24	7.71
1095	5.90	3.19	7.80
4150, Rc14	5.86	2.79	7.84
4150, Rc 18	5.88	3.18	7.82
4150, Rc 43	5.87	3.20	7.81
4150, Rc 64	5.83	2.77	7.80
4340	5.85	3.24	7.80
52100 Annealed	5.99	3.27	7.83
52100 Hardened	5.89	3.20	7.8
D6 Tool Steel Annealed	6.14	3.31	7.7
Stainless Steels			
302	5.66	3.12	7.9
304L	5.64	3.07	7.9
347	5.74	3.10	7.91
410	5.39	2.99	7.67
430	6.01	3.36	7.7
Tantalum	4.10	2.90	16.6
Thorium	2.94	1.56	11.3
Thulium	3.009	1.809	9.29
Tin	3.32	1.67	7.29
Titanium (Ti-6-4)	6.18	3.29	4.50
Tungsten			
Annealed	5.221	2.887	19.25
Drawn	5.410	2.640	19.25
Uranium	3.37	1.98	18.7
Vanadium	6.023	2.774	6.03
Ytterbium	1.946	1.193	6.99
Yttrium	4.10	2.38	4.34
Zinc	4.187	2.421	7.10
Zirconium	4.65	2.25	6.48

Ultrasonic Properties of Solids: Ceramics

Ceramic (20°C unless noted)	Longitudinal Wave Speed × 10 ⁵ cm/sec	Transverse Wave Speed × 10 ⁵ cm/sec	Density gm/cm ³
Aluminum Oxide	10.84	6.36	3.98
Barium Nitrate	4.12	2.28	3.24
Barium Titanate	5.65	3.03	5.5
Bone (Human Tibia)	4.00	1.97	1.7-2.0
Cobalt Oxide	6.56	3.32	6.39
Concrete	4.25-5.25		2.60
Glass			
Crown	5.66	3.42	2.50
Flint	4.26	2.56	3.60
Lead	3.76	2.22	4.6
Plate	5.77	3.43	2.51
Pyrex	5.57	3.44	2.23
Soft	5.40		2.40
Gramite	3.95		2.75
Graphite	4.21	2.03	2.25
Ice (-16°C)	3.83	1.92	0.94
Indium Antimonide	3.59	1.91	
Lead Nitrate	3.28	1.47	4.53
Lithium Fluoride	6.56	3.84	2.64

Ultrasonic Properties of Solids: Ceramics (Continued)

Ceramic (20°C unless noted)	Longitudinal Wave Speed $\times 10^5$ cm/sec	Transverse Wave Speed $\times 10^5$ cm/sec	Density gm/cm ³
Magnesium Oxide	9.32	5.76	3.58
Manganese Oxide	6.68	3.59	5.37
Nickel Oxide	6.60	3.68	6.79
Porcelain	5.34	3.12	2.41
Quartz			
Crystalline	5.73		2.65
Fused	5.57	3.52	2.60
Polycrystalline	5.75	3.72	2.65
Rock Salt	4.60	2.71	2.17
Titanium Dioxide (Rutile)	8.72	4.44	4.26
Sandstone	2.92	1.84	2.2–2.4
Sapphire (c-axis)	11.91	7.66	3.97
Slate	4.50		2.6–3.3
Titanium Carbide	8.27	5.16	5.15
Tourmaline (Z-cut)	7.54		3.10
Tungsten Carbide	6.66	3.98	10.15
Ytterium Iron Garnet	7.29	4.41	5.17
Zinc Sulfide	5.17	2.42	4.02
Zinc Oxide	6.00	2.84	5.61

Ultrasonic Properties of Solids: Polymers

Polymer (20°C unless noted)	Longitudinal Wave Speed $\times 10^5$ cm/sec	Transverse Wave Speed $\times 10^5$ cm/sec	Density gm/cm ³
Acrylic Resin	2.67	1.12	1.18
Bakelite	2.59		1.40
Butyl Rubber	1.99		1.13
Cellulose Acetate	2.45		1.30
Cork	0.5		0.2
Delrin (Acetalhomo-Polymer) (0°C)	2.515		1.42
Ebonite	2.50		1.15
Lexan (Polycarbonate 0°C)	2.28		1.19
Neoprene	1.730		1.42
Nylon	2.68		
Nylon 6,6	1.68		
Parafin	2.20	0.83	
Perspex	2.70	1.33	1.29
Phenolic	1.42		1.34
Plexiglas			
UVA	2.76		1.27
UVA II	2.73	1.43	1.18
Polyacrylonitrile–butadiene– styrene I	2.16	1.43	1.18
Polyacrylonitrile–butadiene– styrene II	2.20	0.810	1.022
Polybutadiene Rubber	1.57		1.10
Polycaprolactam	2.700	1.12	1.146
Polycarboranesiloxane	1.450		1.041
Polydimethylsiloxane	1.020		1.045

Ultrasonic Properties of Solids: Polymers (Continued)

Polymer (20°C unless noted)	Longitudinal Wave Speed × 10 ⁵ cm/sec	Transverse Wave Speed × 10 ⁵ cm/sec	Density gm/cm ³
Polyepoxide + glass spheres I	2.220	1.170	0.691
Polyepoxide + glass spheres II	2.400	1.280	0.718
Polyepoxide + glass spheres III	2.100	1.020	0.793
Polyepoxide + MPDA	2.820	1.230	1.205
Polyester + water	1.840	0.650	1.042
Polythylene	2.67		1.10
Polyhexamethylene adipamide	2.710	1.120	1.147
Polymethacrylate	2.690	1.344	1.191
Polyoxymethylene	2.440	1.000	1.425
Polypropylene	2.650	1.300	0.913
Polystyrene	2.400	1.150	1.052
Polysulfane Resin	2.297		1.24
Polytetrafluoroethylene (Teflon)	1.380		2.177
Polyvinylbutyral	2.350		1.107
Polyvinyl Chloride	2.300		
Polyvinylidene Chloride	2.400		
Polyvinylidene Fluoride	1.930		1.779
Rubber			
India	1.48		0.90
Natural	1.55		1.12
Rubber/Carbon (100/40)	1.68		
Silicon Rubber	0.948		1.48

Calculated Ultrasonic Properties of Composites

Composite (20°C)	Longitudinal Wave Speed × 10 ⁵ cm/sec	Transverse Wave Speed × 10 ⁵ cm/sec	Density gm/cm ³
Glass/Epoxy (parallel to fibers)	5.18	1.63	1.91
Glass/Epoxy (perpendicular to fibers)	3.16	1.72	1.91
Graphite/Epoxy (parallel to fibers)	9.62	1.96	1.57
Graphite/Epoxy (perpendicular to fibers)	2.96	1.96	1.57
Boron/Epoxy (parallel to fibers)	10.60	1.72	1.91
Boron/Epoxy (perpendicular to fibers)	3.34	1.85	1.91

APPENDIX B

ELECTRICAL RESISTIVITIES AND CONDUCTIVITIES OF COMMERCIAL METALS AND ALLOYS

Common Name (Classification)	Resistivity (micro-ohm cm)	Conductivity (% IACS)
Ingot iron (included for comparison)	9	19
Plain carbon steel (AISI-SAE 1020)	10	17
Stainless steel type 304	72	2.4
Cast gray iron (ASTH A48-48, Class 25)	67	2.6
Malleable iron (ASTM A 47)	30	5.7
Ductile cast iron (ASTH A339, A395)	60	2.9
Ni (resist cast iron, type 2)	170	1.0
Cast 28-7 alloy 11D (ASTH A297-63T)	41	4.2
Hastelloy C	139	1.2
Hastelloy X	115	1.5
Haynes Stellite alloy 25	8B	2.0
Inconel X (annealed)	122	1.4
Inconel 600	98	1.7
Aluminum alloy 3003, rolled (ASTH B221)	4	43
Aluminum alloy 2017, annealed (ASTH B221)	4	43
Aluminum alloy 380 (ASTH SC84B)	7.5	23
A# Aluminum alloy		
6061-T-6	4.1	42
7075-T-6	5.3	32
2024-T-4	5.2	30
Copper (ASTH B152, B124, B133, B1, B2, B3)	1.7	1.0×10^2
Yellow brass or high brass (ASTH B36, B134, B135)	7	25
70-30 brass	6.2	28
Aluminum bronze		
ASTH B 169, alloy A	12	14
ASTH B124, B130		
Phosphor bronzes	16	11
Nickel silver I B% alloy A wrought (ASTH B 122, No. 2)	29	5.9
Cupronickel 30%	35	4.9
Red brass, cast (ASTH B30, No. 4A)	11	16
Chemical lead	21	8.2
Antimonial lead (hard lead)	23	7.5
Solder 50-50	15	N
Ti-6Al-4V alloy	172	1.0
Magnesium alloy AZ31 B	9	19
K Monel	58	3.0
Nickel (ASTH B160, B161, B162)	10	17
Cupronickel 55-45 (constantan)	49	3.5
Commercial titanium	80	2.2
Waspaloy	123	1.4
Zinc (ASTH B69)	6	29
Zircaloy-2	72	2.4
Zirconium (commercial)	41	4.2

REFERENCES

1. *The Nondestructive Testing Handbooks*, 2nd ed., American Society for Nondestructive Testing, Columbus, OH: Vol. 1, *Leak Testing*, R. C. McMaster (ed.); Vol. 2, *Liquid Penetrant Testing*, R. C. McMaster (ed.); Vol. 3, *Radiography and Radiation Testing*, L. E. Bryant (ed.); Vol. 4, *Electromagnetic Testing*, M. L. Mester (ed.); Vol. 5, *Acoustic Emission*, R. K. Miller (ed.); Vol. 6, *Magnetic Particle Testing*, J. T. Schmidt and K. Skeie (eds.); Vol. 7, *Ultrasonic Testing*, A. S. Birks and R. E. Green, Jr. (eds.); Vol. 8, *Visual and Optical Testing*, M. W. Allgaier and S. Ness (eds.); Vol. 9, *Special Nondestructive Testing Methods*, R. K. Stanley (ed.).
2. D. E. Bray and R. K. Stanley, *Nondestructive Evaluation, A Tool for Design, Manufacturing, and Service*, McGraw-Hill, New York, 1989.
3. R. Halmshaw, *Nondestructive Testing Handbook*, 2nd ed., Chapman & Hall, London, 1991.
4. *Metals Handbook: Nondestructive Evaluation and Quality Control*, Vol. 11, American Society for Metals, Metals Park, OH, 1976.
5. R. A. Kline, *Nondestructive Characterization of Materials*, Technomic, Lancaster, PA, 1992.
6. *Annual Book of ASTM Standards: Part II, Metallography and Nondestructive Testing*, American Society for Testing and Materials, Philadelphia, PA.
7. *Materials Evaluation*, American Society for Nondestructive Testing, Columbus, OH.
8. *British Journal of Nondestructive Testing*, British Institute of Nondestructive Testing, Northampton, UK.
9. *NDT International*, IPC Business Press Ltd., Sussex, UK.
10. *Non-Destructive Testing Journal*, Energitechnik, Japan (c/o Japan Technical Services Corp., 3F Ohkura Bldg., 4-10 Shiba-Daimon 1 Chrome, Mitato-ku Tokyo, 105, JAPAN).
11. *Soviet Journal of Nondestructive Testing*, translated by Consultants Bureau, New York.
12. *Journal of Nondestructive Testing*, Plenum Press, New York.
13. K. Ono (ed.), *Journal of Acoustic Emission*, Plenum Press, New York.
14. *Sensors—The Journal of Machine Perception*, Halmers Publishing, Peterborough, NH.
15. J. Krautkramer and H. Krautkramer, *Ultrasonic Testing of Materials*, 4th ed., Springer-Verlag, New York, 1995.
16. R. A. Quinn, *Industrial Radiology—Theory and Practice*, Eastman Kodak, Rochester, NY, 1980.
17. H. Burger, *Neutron Radiography: Methods, Capabilities and Applications*, Elsevier, New York, 1965.
18. F. Förster, "Theoretische und experimentelle Grundlagen der zerstörungsfreien Werkstoffprüfung mit Wirbelstromverfahren. I. Das Tastpulverfahren," *Z. Metallk.* **43**, 163–171 (1952).